

Key factors affecting graphene oxide transport in saturated porous media

*Original*

Key factors affecting graphene oxide transport in saturated porous media / Beryani, Ali; Alavi Moghaddam, M. R.; Tosco, T.; Bianco, C.; Hosseini, S. M.; Kowsari, E.; Sethi, R.. - In: SCIENCE OF THE TOTAL ENVIRONMENT. - ISSN 0048-9697. - 698:(2020), p. 134224. [10.1016/j.scitotenv.2019.134224]

*Availability:*

This version is available at: 11583/2784318 since: 2020-01-23T10:24:42Z

*Publisher:*

Elsevier B.V.

*Published*

DOI:10.1016/j.scitotenv.2019.134224

*Terms of use:*

This article is made available under terms and conditions as specified in the corresponding bibliographic description in the repository

*Publisher copyright*

(Article begins on next page)

# Key factors affecting graphene oxide transport in saturated porous media

Ali Beryani<sup>(1)(a)</sup>, Mohammad Reza Alavi Moghaddam<sup>(1)(\*)</sup>, Tiziana Tosco<sup>(2)</sup>, Carlo Bianco<sup>(2)</sup>, Seiyed Mossa Hosseini<sup>(3)</sup>, Elaheh Kowsari<sup>(1)</sup>, Rajandrea Sethi<sup>(2)</sup>

(1) Department of Civil and Environmental Engineering (CEE), Amirkabir University of Technology, Hafez Ave., 424, 15875-4413, Tehran, Iran

(2) Department of Environmental, Land and Infrastructure Engineering, Politecnico di Torino, Corso Duca degli Abruzzi 24 10129, Torino, Italy

(3) Physical Geography Department, University of Tehran, 16th Azar St., Enghelab Sq., 14155-6465, Tehran, Iran.

(a) Present address: Department of Environmental, Land and Infrastructure Engineering, Politecnico di Torino, Corso Duca degli Abruzzi 24 10129, Torino, Italy

(\*) Corresponding author: alavi@aut.ac.ir, alavim@yahoo.com, tel. +98 021 64543008

Revised manuscript submitted to

Science of the Total Environment

July 2019

26

## Abstract

27

This study focuses on the transport in porous media of graphene oxide nanoparticles (GONP) under conditions similar to those applied in the generation of *in-situ* reactive zones for groundwater remediation (i.e. GO concentration of few tens of mg/l, stable suspension in alkaline solution). The experimental tests evaluated the influence on GO transport of three key factors, namely particle size (300–1200 nm), concentration (10–50 mg/L), and sand size (coarse to fine). Three sources of GONP were considered (two commercial and one synthesized in the laboratory). Particles were stably dispersed in water at pH 8.5 and showed a good mobility in the porous medium under all experimental conditions: after injection of 5 pore volumes and flushing, the highest recovery was around 90%, the lowest around 30% (only for largest particles in fine sand). The particle size was by far the most impacting parameter, with increasing mobility with decreasing size, even if sand size and particle concentration were also relevant. The source of GONP showed a minor impact on the mobility. The transport test data were successfully modeled using the advection-dispersion-deposition equations typically applied for spherical colloids. Experimental and modeling results suggested that GONP, under the explored conditions, are retained due to both blocking and straining, the latter being relevant only for large particles and/or fine sand. The findings of this study play a key role in the development of an *in-situ* groundwater remediation technology based on the injection of GONP for contaminant degradation or sorption. Despite their peculiar shape, GONP behavior in porous media is comparable with spherical colloids, which have been more studied by far. In particular, the possibility of modeling GONP transport using existing models ensures that they can be applied also for the design of field-scale injections of GONP, similarly to other particles already used in nanoremediation.

49

50

51

### Keywords:

52

Graphene oxide, transport in porous media, nanoparticle size effect, blocking, straining, nanoremediation

53

54

55

### Highlights:

56

Graphene oxide transport is controlled by blocking and straining phenomena

57

Graphene oxide mobility in porous media strongly depends on its lateral size

58

A power law correlates the attachment/detachment coefficients to GO particle size

59

Good mobility/stability of GO makes it potentially capable in groundwater remediation

60

61

62

63  
64  
65  
66  
67  
68  
69  
70  
71  
72  
73  
74  
75  
76  
77  
78  
79  
80  
81  
82  
83  
84  
85  
86

## 1. Introduction

Graphene oxide nanoparticles (GONP) are carbon-based irregular 2D flakes with a nanoscale thickness (Chen et al., 2012). GONP contain large amounts of oxygenated functional groups at the surface, such as carbonyl, carboxyl, hydroxyl, and phenol (Huang et al., 2011). They have been studied for several, diverse applications, e.g. in electronics, biomedicine, and sensors (Liu et al., 2013a; Novoselov et al., 2012; Qi et al., 2014a; Tortello et al., 2016). More recently, laboratory studies showed that GO can effectively remove several organic contaminants (Akpotu and Moodley, 2018; Iqbal and Abdala, 2013; Yang et al., 2013) and heavy metals (Jiang et al., 2018; Yin et al., 2019; Zhao et al., 2019; Zhou et al., 2016) from contaminated water. This evidence opens perspectives for several environmental applications, including wastewater treatment and in-situ remediation of contaminated aquifer systems, in particular for the removal of recalcitrant compounds and specific contaminants of concerns.

For the in-situ remediation the reference technology is the nanoremediation, that is, the injection of nanoparticles into the contaminated aquifer system for degradation, sorption precipitation or complexation of organic or inorganic contaminants (Corsi et al., 2018; Karn et al., 2009; O'Carroll et al., 2013; Patil et al., 2016; Tosco et al., 2014). The reactive particles must be dispersed and stably suspended in water-based slurries, thus allowing effective injection and targeting of the treatment area, which can be accomplished only with a strong control of the particle mobility in the porous medium. As a consequence, it is of pivotal importance to understand the main operative parameters controlling particle transport in the porous medium, and to develop reliable transport models to predict the particle mobility during injection and the final distribution of the reactive material. In this work, we study at a laboratory scale the potential injectability of GONP in the subsurface, which is a crucial aspect for the use of any nanoparticle for in situ treatment of a contaminated aquifer. In particular,

87 we study how GONP transport in porous media is affected by those parameters which usually  
88 play a key role in nanoparticle injection for groundwater remediation, namely particle size  
89 and concentration, and porous medium size.

90 Compared to other materials already used for nanoremediation, eg. zero valent iron NPs,  
91 GONP inherently possess negative charges under a wide range of different environmental  
92 conditions, and can be easily dispersed in aqueous solutions, remaining suspended for a long  
93 period, even in the absence of stabilizers (Liu et al., 2013b; Qi et al., 2014a). Moreover, up to  
94 now most studies demonstrated that GONP tend to poorly interact with the porous medium,  
95 and therefore are retained on sand grains in limited amounts (Dong et al., 2016; Fan et al.,  
96 2015a; Feriencikova and Xu, 2012; Lanphere et al., 2013; Liu et al., 2013a; Liu et al., 2013c;  
97 Qi et al., 2014a; Sun et al., 2015; Xia et al., 2019). Thus, previous studies suggest a good  
98 potential mobility of GONP in aquifers and a relatively easy injectability at the field scale,  
99 compared to other nanoparticles already employed in the nanoremediation.

100 Until now, studies have been published on the suspension stability, transport and retention of  
101 GONP in porous media (Lanphere et al., 2014; Li et al., 2016; Liu et al., 2013b; Wang et al.,  
102 2017). However, they mostly focused on the influence of solution chemical parameters such  
103 as pH, ionic strength (IS), ion valence, and natural organic matter (NOM) concentration,  
104 which all play a key role on the long term fate of GONP in aquifer systems (Chrysikopoulos  
105 et al., 2017; Fan et al., 2015a; Fan et al., 2015b; Feriencikova and Xu, 2012; Jian-Zhou et al.,  
106 2015; Lanphere et al., 2013; Liu et al., 2013b; Liu et al., 2013c; Lu et al., 2017; Peng et al.,  
107 2017; Qi et al., 2014a; Xia et al., 2019). In particular, the influence of ion concentration and  
108 valence is now relatively well understood. Conversely, in this work we focus mainly on  
109 particle size and concentration and their physical interactions with porous media of different  
110 grain size; all these parameters become extremely relevant when particle suspensions are  
111 injected on purpose in the subsoil.

112 Particle size is known to play a critical role in colloid transport, as already elucidated by a  
113 broad literature, from colloid filtration theory and beyond. The porous medium grain size can  
114 have a huge impact on the colloid transport and retention, as predictable by the colloidal  
115 filtration theory (CFT) (Tufenkji and Elimelech, 2004; Yao et al., 1971). However, a direct  
116 extension of known processes and modeling approaches to GONP is not necessarily  
117 straightforward, due to the peculiar shape of such platelets. To the authors' knowledge, no  
118 previous study has already investigated and quantified the influence of particle size on GONP  
119 transport, and a few studies (Dong et al., 2019; Sun et al., 2012) have investigated the grain  
120 size effect on the transport and retention of GONP. Also, there is a lack of systematic  
121 information about the relationship between size of plate-like nanoparticles and their retention  
122 kinetic parameters. In this study, we consequently develop empirical equations expressing  
123 this relationship.

124 As a general rule, when colloidal suspensions are fairly stable and particles are sufficiently  
125 small compared to pore size to avoid straining and filtration phenomena, the injected  
126 concentration has a limited impact on particle transport, which is dominated by blocking  
127 phenomena (Tosco et al., 2014). This is the case of colloidal suspensions like bacteria,  
128 carboxylic latex, silica, titania and silver nanoparticles, and carbon nanotubes (Bradford and  
129 Bettahar, 2006; Bradford et al., 2009; Camesano and Logan, 1998; Godinez and Darnault,  
130 2011; Kasel et al., 2012; Liang et al., 2013; Wang et al., 2012; Zhang et al., 2010). When  
131 considering the injection of particle suspensions for nanoremediation, graphene oxide is  
132 expected to be injected in relatively high concentrations (eg. several tens of mg/L) and then  
133 diluted in groundwater. In these conditions, the injected concentration often plays a major role  
134 in particle mobility and distribution in the porous medium. Sun et al. (2015) found that GONP  
135 mobility into sand-packed columns increased at higher input concentrations, coherently with  
136 the good colloidal stability of graphene oxide suspensions. In the present work, the impact of

137 the injected concentration on GONP mobility is further studied, extending the range of  
138 conditions explored in the cited study.

139 In light of what discussed above, the aim of the present research is to elucidate unexplored or  
140 still unclear aspects related to GONP transport in porous media under conditions which could  
141 be expected for its application in nanoremediation, and to provide a reliable modeling  
142 framework able to correctly reproduce the observed processes. Column transport tests were  
143 performed using different graphene oxide types, particle size, injected concentration and sand  
144 samples. The experimental results were modeled using a well-established advection-  
145 dispersion-deposition equation for particle transport, using the numerical solution provided  
146 by the software MNMs (Bianco et al., 2016). Afterwards, the dependence of the model  
147 coefficients on the abovementioned parameters was quantified.

148

## 2. Materials and methods

### 2.1. GONP suspensions

In this study, three types of graphene oxide were used, identified as GO<sub>1</sub>, GO<sub>2</sub>, and GO<sub>3</sub> (Table 1). GO<sub>1</sub> (Graphenea Inc., Spain) is a single-layer graphene oxide dispersion, provided in a concentrated stock solution (4 g/L). GO<sub>2</sub> (Cheap Tubes Inc., US) is a single-layer GO provided in a dry powder ;from ,a stock solution (2 g/L) was then prepared by suspending the particles in DI water. GO<sub>3</sub> was synthesized in the laboratory following an eco-friendly improved Hummer's method developed by Chen et al. (2013), and stored in a stock solution at 1.45 g/L.

The synthesized GO<sub>3</sub> was characterized into details using the following methods: energy-dispersive X-ray spectroscopy (EDX, Octane SDD equipped with the SUTW detector, EDAX, United States), Fourier transform infrared spectroscopy (FT-IR, Bruker FTIR Equinox 55 spectroscopy, equipped with a MCT cryo-detector, Germany), X-ray diffraction (XRD, Equinox 3000, Inel, United States), Atomic Force Microscopy (AFM, NTEGRA AFMNT-MDT, NT-MDT Spectrum Instruments, Russia), and Field Emission Scanning Electron Microscopy (FE-SEM, Supra 40, ZEISS, Germany). The results of the characterization are reported in the Supporting Information. For the commercial GO<sub>1</sub> and GO<sub>2</sub> samples similar analyses were provided by the manufacturers (see SI for references).

Table 1: Characteristics of GO<sub>1</sub>, GO<sub>2</sub>, and GO<sub>3</sub>

Name	Producer	Synthesis method	Size range after sonication (μm) (*)	Number of layers (**)	Thickness of layers (nm) (**)	Elemental analysis (***)			
						Carbon % (w/w)	Oxygen % (w/w)	Hydrogen % (w/w)	Sulfur % (w/w)
GO <sub>1</sub>	Graphenea	Modified Hummer's method	0.3-1.6	1	0.8~1.2	49-56	41-50	0-1	2-4
GO <sub>2</sub>	Cheap Tubes	Modified Hummer's method	0.3-0.8	1	0.7~1.2	35-42	45-55	3-5	-
GO <sub>3</sub>	Own synthesis	Improved Hummer's method (without using NaNO <sub>3</sub> )	0.9-1.5	1-2	0.8~2	45-60	40-55	-	<1
(*) DLS measurements (**) AFM analysis for GO <sub>3</sub> , manufacturers' data sheets for GO <sub>1</sub> and GO <sub>2</sub> (***) EDX analysis for GO <sub>3</sub> , manufacturers' data sheets for GO <sub>1</sub> and GO <sub>2</sub>									

168

169 Size and zeta potential measurements were performed using dynamic light scattering (DLS)  
 170 (Zetasizer Nano ZSP, Malvern Instruments, UK) for the three GO types.

171 For all tests, the GONP suspension was prepared immediately before injection by: diluting  
 172 the stock solution to the desired GO concentration with DI water, applying probe sonication  
 173 (UP200s Hielscher Ultrasound Technology, Germany), adding NaCl and NaOH to adjust,  
 174 respectively, ionic strength (20 mM) and pH (8.5±0.5), and degassing in a vacuum chamber  
 175 to remove residual air micro-bubbles. For GO<sub>1</sub> and GO<sub>3</sub>, a different sonicating duration was  
 176 used to adjust the average size of the particles (see detailed discussion on paragraph 3.1) and  
 177 for GO<sub>2</sub> a 5 mins sonication was performed. The pH value was selected as typical value for  
 178 GONP suspensions with good colloidal stability, which is therefore expected to be used in  
 179 case of GO application to groundwater nanoremediation.

180

## 2.2. Porous medium

181 Silica sand with a minor content of K-feldspar (Sibelco, Dorfner, Germany) was sieved to  
 182 obtain three different size ranges: coarse S<sub>1</sub> (0.3~1.0 mm, d<sub>50</sub>=0.75 mm), medium S<sub>2</sub> (0.25~0.5  
 183 mm, d<sub>50</sub>=0.4 mm), and fine S<sub>3</sub> (0.075~0.6 mm, d<sub>50</sub>=0.28 mm). Prior to column packing, to

184 remove fine suspended solids, metal oxides and other possible impurities, the sand was  
185 cleaned following the procedure reported in (Liu et al., 2013b; Qi et al., 2014a; Sun et al.,  
186 2015; Tosco et al., 2009). The zeta potential of the sand was measured (Zetasizer Nano ZSP,  
187 Malvern) following the method developed by Johnson et al. (1996). The measured values of  
188 zeta potential were  $-38\pm 2$ ,  $-40\pm 1$  and  $-42\pm 2$  mV for S<sub>1</sub>, S<sub>2</sub>, and S<sub>3</sub> in 20 mM NaCl solution at  
189 pH 8.5, respectively.

### 191 2.3. GONP transport tests

192 A Plexiglas cylinder (length 15.2 cm, inner diameter 1.6 cm) was wet-packed with degassed  
193 sand following the protocol detailed by Tosco et al. (2012). The column experiments were  
194 performed at a constant injection rate of  $1.63\times 10^{-8}$  m<sup>3</sup>/s, resulting in a Darcy velocity of  
195  $8.11\times 10^{-5}$  m/s. GONP suspensions were prepared following the protocol described in  
196 paragraph 2.1 at concentrations of 50, 20, 15 and 10 mg/L, representative of GONP  
197 concentrations applicable for field injections. The injection protocol involved the following  
198 steps:

- 199 - Pre-equilibration of the column with DI water for 5 pore volumes (PVs);
- 200 - Pre-flushing with background electrolyte solution (NaCl 20 mM) for 5 PVs;
- 201 - Injection of the GONP suspension in the background electrolyte solution for 4.5 PVs;
- 202 - Flushing with the background electrolyte solution for 4 PVs;
- 203 - Final flushing with DI water for 5 PVs (only for selected column tests).

204 During the experiments, salt and GONP concentrations were continuously measured at the  
205 column inlet and outlet using an UV-Vis Spectrophotometer (Specord S600, Analytik Jena,  
206 Germany) equipped with flow-through quartz cells with 5 mm light path (Hellma, Germany).  
207 The concentration was continuously monitored at a measurement frequency of 10 seconds at  
208 wavelengths of 198 nm (for dissolved species) and 230 nm (for GONP).

For each column test, the effective porosity ( $\epsilon$ ) and the dispersivity ( $\alpha$ ) were determined via inverse fitting of the NaCl breakthrough curve (BTC), according to (Bianco et al., 2016). An average effective porosity of 0.49( $\pm$ 0.015), 0.47( $\pm$ 0.005), and 0.44( $\pm$ 0.015) and an average dispersivity of 5.16( $\pm$ 0.784) $\times 10^{-4}$  m, 4.87( $\pm$ 0.589) $\times 10^{-4}$  m, and 3.97( $\pm$ 0.813) $\times 10^{-4}$  m were obtained for the sands S<sub>1</sub>, S<sub>2</sub>, and S<sub>3</sub>, respectively. The detailed results for each column test are reported in Table S1.

At the end of each column test, the sand column was dissected into five sections of 3 cm each to determine the profiles of retained GO mass and average particle size. The dissection procedure and the validation of concentration profiles against breakthrough curve mass balances are detailed in SI.

The GONP column transport tests were performed using different combinations of GO type (GO<sub>1</sub>, GO<sub>2</sub>, and GO<sub>3</sub>), size and concentration, as well as different sand average size to systematically investigate the influence of these parameters on the transport of GONP.

#### 2.4. GONP transport and retention modeling

The transport and retention of GONP in 1D saturated porous media was modeled using the general formulation of the advection-dispersion equation modified to include the particle mass exchange (deposition and release) between liquid and solid phase (Bradford and Bettahar, 2006; Bradford et al., 2003; Hosseini and Tosco, 2013; Qi et al., 2014a; Qi et al., 2014b; Tosco and Sethi, 2010; Wang et al., 2011) implemented in MNMs (<https://areeweb.polito.it/ricerca/groundwater/software>):

$$\begin{cases} \frac{\partial}{\partial t}(\epsilon C) + \sum_i \left( \rho_b \frac{\partial S_i}{\partial t} \right) = - \frac{\partial}{\partial x}(qC) + \frac{\partial}{\partial x} \left( \epsilon D \frac{\partial C}{\partial x} \right) \\ \rho_b \frac{\partial S_i}{\partial t} = f_i(C, S_i) = \epsilon k_{a,i} \psi_i C - \rho_b k_{d,i} S_i \end{cases} \quad (\text{eq. 3})$$

231 where  $C$  is the concentration of the nanoparticles in the liquid phase [ $M L^{-3}$ ],  $t$  is time [ $T$ ],  $\epsilon$   
 232 is the medium porosity [-],  $i$  is a subscript regarding to the  $i^{\text{th}}$  interaction site,  $\rho_b$  is the bulk  
 233 density of the porous medium [ $M L^{-3}$ ],  $S_i$  is the mass concentration of nanoparticles deposited  
 234 on the  $i^{\text{th}}$  site [ $M M^{-1}$ ],  $x$  is the distance traveled from the inlet [ $L$ ],  $q$  is Darcy flow rate [ $L T^{-1}$ ],  
 235  $D$  is the dispersion coefficient [ $L^2 T^{-1}$ ],  $k_{a,i}$  and  $k_{d,i}$  are the attachment and detachment  
 236 kinetic coefficients, respectively [ $T^{-1}$ ], and  $\psi_i$  is a function controlling the interaction  
 237 dynamics of colloid deposition for  $i^{\text{th}}$  site.

238 In this study, a 2-site model considering two interaction mechanisms was used to describe  
 239 particle interactions with the porous medium, namely, a physico-chemical  
 240 attachment/detachment site with a maximum retainable concentration  $S_{\max,1}$  [ $M M^{-1}$ ]  
 241 (reversible blocking site,  $i=1$ ) and a second site describing the physical retention of the  
 242 nanoparticles (irreversible straining site,  $i=2$ ). For the second interaction mechanism, the  
 243 formulation proposed by Bradford et al. (2004; 2003) was adopted:

$$244 \quad \psi_1 = \left(1 - \frac{S_1}{S_{\max,1}}\right) \quad (\text{eq.2})$$

$$245 \quad \psi_2 = \left(1 + \frac{x}{d_{50}}\right)^{\beta_{str,2}} \quad (\text{eq.3})$$

246 where  $d_{50}$  is the mean size of sand grains [ $L$ ], and  $\beta_{str,2}$  [-] is a kinetic exponent controlling the  
 247 shape of the spatial distribution of retained nanoparticles.

248 The experimental breakthrough curves (BTCs) of GONP were fitted to the mathematical  
 249 model using MNMs. The fitting parameters include the attachment/detachment kinetics ( $k_{a,1}$ ,  
 250  $k_{d,1}$ ,  $k_{a,2}$ ) and the maximum retainable concentration  $S_{\max,1}$ . The exponent  $\beta_{str,2}$  was assumed  
 251 equal to the value proposed in the literature (0.432) with good results (Bradford et al., 2003).

### 252 **3. Results and discussions**

#### 253 **3.1. Characterization of synthesized GONP (GO<sub>3</sub>)**

254 EDX analysis indicated that GO<sub>1</sub> and GO<sub>3</sub> contain similar percentages of C and O (Table 1).  
255 For GO<sub>2</sub> the produce reports a slightly higher content of C and lower of O. FT-IR transmission  
256 spectra confirmed for GO<sub>3</sub> the existence of epoxide (–O–), carbonyl (–C=O), carboxyl (–  
257 COOH) and hydroxyl (–OH) functional groups on the GO<sub>3</sub> surface (Figure S2). The XRD  
258 pattern of dried GO<sub>3</sub> showed a reflection peak at  $2\theta=12^\circ$ , corresponding to d-space of 0.741  
259 nm (Figure S3). This large interlayer spacing between the sheets implies the existence of  
260 oxygenated functional groups produced by the harsh chemical oxidation of pure graphite  
261 (with the smaller initial d-spacing of about 0.3 nm) and the formation of graphene oxide (Chen  
262 et al., 2013; Paulchamy et al., 2015; Shahriary and Athawale, 2014).

263 The specific surface area of the GO<sub>3</sub> (989 m<sup>2</sup>/g) was estimated using the methylene blue  
264 titration method proposed by Montes-Navajas et al. (2013). The experimental procedure and  
265 calculations of specific surface area are detailed in the SI (Figure S4).

266 AFM analysis indicated that the synthesized GO<sub>3</sub> suspension (in DI, after 45 seconds ultra-  
267 sonication) consisted of single- or two-layer flakes with thickness 0.8~2 nm (Figure S5) and  
268 lateral size of 500~1000 nm. AFM analysis of GO<sub>2</sub> provided by the manufacturer evidenced  
269 a similar thickness (up to 3 nm). FE-SEM analysis also showed that the lateral size of GO<sub>3</sub>  
270 after synthesis (without size adjustment) ranged between 900~1500 nm (Figure S6).

271 GONP formed stable colloidal suspensions: kinetic aggregation measurements using DLS  
272 (Figure S7) and visual sedimentation tests (not reported) indicated that the three GONP were  
273 all stably dispersed in a 20 mM NaCl solution for at least two hours (i.e. longer than the  
274 duration of the transport tests). This is in agreement with the strongly negative values of Zeta  
275 potential measured for the suspensions ( $-50\pm 4$ ,  $-55\pm 6$ , and  $-56\pm 1$  mV for GO<sub>1</sub>, GO<sub>2</sub>, and GO<sub>3</sub>,  
276 respectively).

277 It was observed that applying probe sonication for a different duration the average size of the  
278 GONP in suspension changes: the longer the duration, the smaller the average size (Figure

279 S8). Particle size distribution is broader if no sonication is applied, or applied for short  
280 durations, and becomes narrower when sonication is prolonged (3 mins or higher). Sonication  
281 did not significantly alter other properties of the GONP (colloidal stability and zeta potential,  
282 compare Figure S9). Consequently, based on these results, the average size of GO<sub>1</sub> and GO<sub>3</sub>  
283 (Table 2) was controlled by changing the duration of probe sonication during the suspension  
284 preparation, following Figure S8.

285 It is worth to mention that, due to their platelet-like shape, GONP size measurements obtained  
286 from DLS cannot be directly interpreted as the correct size of the particles, and are rather  
287 related to both platelet lateral size, shape and thickness, as discussed in the literature (Lotya  
288 et al., 2013). Consequently, in this work the measured average size values were used as a  
289 semi-quantitative measurement of the lateral size, and changes in average size were analyzed  
290 mainly in terms of particle size increase/decrease, rather than absolute values. The actual  
291 lateral size was instead obtained from SEM and AFM measurements (see Supporting  
292 Information).

### 293 **3.2. Column transport tests**

294 The GONP column transport tests were performed using different combinations of GO type  
295 (GO<sub>1</sub>, GO<sub>2</sub>, and GO<sub>3</sub>), lateral size and concentration, as well as different sand average size to  
296 systematically investigate the influence of these parameters on the transport of graphene oxide  
297 (Table 2). The observed and simulated BTCs were normalized to the injected concentration  
298 ( $C/C_0$ ) and reported as a function of pore volumes (Figure 1, Figure 4, and Figure 6). In the  
299 graphs, P.V. = 0 (time  $t = 0$ ) corresponds to the beginning of GO injection, thus equilibration  
300 and pre-flushing steps are not reported. The retention profiles were reported as a normalized  
301 concentration of deposited GONP ( $S$ , namely mass of GONP normalized to the sand mass)  
302 (Figure 2, Figure 5, and Figure 7).

303 The experimental BTCs were fitted using the 2-site retention model equations (1-3). As a  
304 general rule, the results indicated that under the tested experimental conditions the model  
305 equations can satisfactorily simulate the observed BTCs of GONP (for all the experiments  
306  $R^2 > 0.99$ ) with a very little mismatch in both rising and tailing parts of the BTCs. For  $GO_2$   
307 only, in some cases, the second site (straining) had a negligible effect on the particle transport  
308 and was therefore removed. The fitted model parameters are summarized in Table 2.

309 The low values of  $k_{d,1}$  (detachment coefficient for blocking deposition) obtained for all the  
310 tests indicated that physico-chemical deposition will be practically irreversible if the ionic  
311 strength (and therefore the particle-collector electrostatic interactions) is not modified. This  
312 is coherent with the negligible tailing observed in the experimental breakthrough curves. A  
313 few additional tests were performed flushing the columns after particle deposition with  
314 stepwise decreasing salt concentration. The results (Figure S10) revealed that particles  
315 retained due to physical-chemical interactions are not readily mobilized unless a strong  
316 decrease in salt concentration is applied (in our experiments, NaCl concentration below 5  
317 mM).

321

Table 2: Experimental conditions of column transport tests and fitted coefficients ( $k_{a,1}$ ,  $k_{d,1}$ ,

322

 $S_{max,1}$ , and  $k_{a,2}$ )

Test No.	GO Type	C <sub>0</sub> (mg/L)	GO Size (nm)	Sand	k <sub>a,1</sub> [s <sup>-1</sup> ]	k <sub>d,1</sub> [s <sup>-1</sup> ]	S <sub>max,1</sub> [g/g]	k <sub>a,2</sub> [s <sup>-1</sup> ]
1	GO <sub>1</sub>	50	898±47	Coarse	6.06·10 <sup>-4</sup>	8.34·10 <sup>-5</sup>	5.38·10 <sup>-6</sup>	4.70·10 <sup>-4</sup>
2		50	1000±49	Medium	1.20·10 <sup>-3</sup>	8.18·10 <sup>-6</sup>	4.79·10 <sup>-6</sup>	1.90·10 <sup>-3</sup>
3		50	984±55	Fine	2.30·10 <sup>-3</sup>	3.54·10 <sup>-5</sup>	9.00·10 <sup>-6</sup>	3.10·10 <sup>-3</sup>
4		20	1128±111	Coarse	9.07·10 <sup>-4</sup>	5.00·10 <sup>-5</sup>	3.25·10 <sup>-6</sup>	1.40·10 <sup>-3</sup>
5		20	1100±63	Medium	2.50·10 <sup>-3</sup>	3.20·10 <sup>-5</sup>	5.36·10 <sup>-6</sup>	2.40·10 <sup>-3</sup>
6		20	1076±59	Fine	2.44·10 <sup>-3</sup>	2.92·10 <sup>-5</sup>	4.90·10 <sup>-6</sup>	5.28·10 <sup>-3</sup>
7		15	1122±72	Fine	2.90·10 <sup>-3</sup>	1.81·10 <sup>-5</sup>	4.93·10 <sup>-6</sup>	6.20·10 <sup>-3</sup>
8		10	1082±69	Fine	3.60·10 <sup>-3</sup>	5.47·10 <sup>-5</sup>	3.46·10 <sup>-6</sup>	8.90·10 <sup>-3</sup>
9		20	1286±332	Fine	4.08·10 <sup>-3</sup>	2.34·10 <sup>-5</sup>	4.72·10 <sup>-6</sup>	9.30·10 <sup>-3</sup>
10		20	980±40	Fine	2.51·10 <sup>-3</sup>	3.46·10 <sup>-5</sup>	5.44·10 <sup>-6</sup>	5.70·10 <sup>-3</sup>
11		20	820±70	Fine	1.88·10 <sup>-3</sup>	3.49·10 <sup>-5</sup>	4.87·10 <sup>-6</sup>	2.63·10 <sup>-3</sup>
12		20	595±30	Fine	1.70·10 <sup>-3</sup>	4.60·10 <sup>-5</sup>	5.34·10 <sup>-6</sup>	8.95·10 <sup>-4</sup>
13		20	530±30	Fine	1.64·10 <sup>-3</sup>	5.50·10 <sup>-5</sup>	5.56·10 <sup>-6</sup>	9.87·10 <sup>-4</sup>
14		20	380±20	Fine	1.60·10 <sup>-3</sup>	5.80·10 <sup>-5</sup>	4.23·10 <sup>-6</sup>	7.27·10 <sup>-4</sup>
15	GO <sub>2</sub>	50	417±15	Coarse	9.50·10 <sup>-4</sup>	5.64·10 <sup>-5</sup>	9.88·10 <sup>-6</sup>	3.73·10 <sup>-4</sup>
16		50	388±20	Medium	1.30·10 <sup>-3</sup>	6.33·10 <sup>-5</sup>	8.20·10 <sup>-6</sup>	6.82·10 <sup>-4</sup>
17		50	380±8	Fine	2.61·10 <sup>-3</sup>	1.02·10 <sup>-5</sup>	1.38·10 <sup>-5</sup>	1.40·10 <sup>-3</sup>
18		20	362±21	Coarse	1.60·10 <sup>-3</sup>	5.09·10 <sup>-5</sup>	5.79·10 <sup>-6</sup>	-
19		20	393±14	Medium	8.64·10 <sup>-4</sup>	3.41·10 <sup>-5</sup>	4.48·10 <sup>-6</sup>	-
20		20	370±16	Fine	2.75·10 <sup>-3</sup>	2.45·10 <sup>-5</sup>	1.12·10 <sup>-5</sup>	-
21		15	448±54	Fine	2.70·10 <sup>-3</sup>	1.80·10 <sup>-5</sup>	1.07·10 <sup>-5</sup>	-
22		10	409±44	Fine	4.25·10 <sup>-3</sup>	1.34·10 <sup>-5</sup>	8.98·10 <sup>-6</sup>	-
23	GO <sub>3</sub>	50	687±24	Coarse	7.76·10 <sup>-4</sup>	1.13·10 <sup>-4</sup>	8.41·10 <sup>-6</sup>	5.43·10 <sup>-5</sup>
24		50	679±19	Medium	1.10·10 <sup>-3</sup>	8.22·10 <sup>-5</sup>	8.15·10 <sup>-6</sup>	9.82·10 <sup>-4</sup>
25		50	727±28	Fine	2.10·10 <sup>-3</sup>	4.60·10 <sup>-5</sup>	8.04·10 <sup>-6</sup>	1.90·10 <sup>-3</sup>
26		20	650±15	Coarse	1.10·10 <sup>-3</sup>	4.03·10 <sup>-5</sup>	4.83·10 <sup>-6</sup>	1.50·10 <sup>-3</sup>
27		20	677±21	Medium	1.80·10 <sup>-3</sup>	3.51·10 <sup>-5</sup>	7.03·10 <sup>-6</sup>	1.40·10 <sup>-3</sup>
28		20	733±43	Fine	1.90·10 <sup>-3</sup>	4.04·10 <sup>-5</sup>	4.37·10 <sup>-6</sup>	3.70·10 <sup>-3</sup>
29		15	645±27	Fine	3.60·10 <sup>-3</sup>	5.47·10 <sup>-6</sup>	3.46·10 <sup>-6</sup>	8.90·10 <sup>-3</sup>
30		10	588±28	Fine	4.60·10 <sup>-3</sup>	1.02·10 <sup>-5</sup>	5.45·10 <sup>-6</sup>	8.40·10 <sup>-3</sup>
31		20	1167±111	Fine	2.80·10 <sup>-3</sup>	2.74·10 <sup>-5</sup>	6.24·10 <sup>-6</sup>	8.60·10 <sup>-3</sup>
32		20	868±41	Fine	2.00·10 <sup>-3</sup>	3.44·10 <sup>-5</sup>	5.65·10 <sup>-6</sup>	3.30·10 <sup>-3</sup>
33		20	450±15	Fine	1.49·10 <sup>-3</sup>	4.82·10 <sup>-5</sup>	5.21·10 <sup>-6</sup>	1.09·10 <sup>-3</sup>
34		20	270±60	Fine	1.30·10 <sup>-3</sup>	6.33·10 <sup>-5</sup>	4.36·10 <sup>-6</sup>	8.71·10 <sup>-4</sup>

323

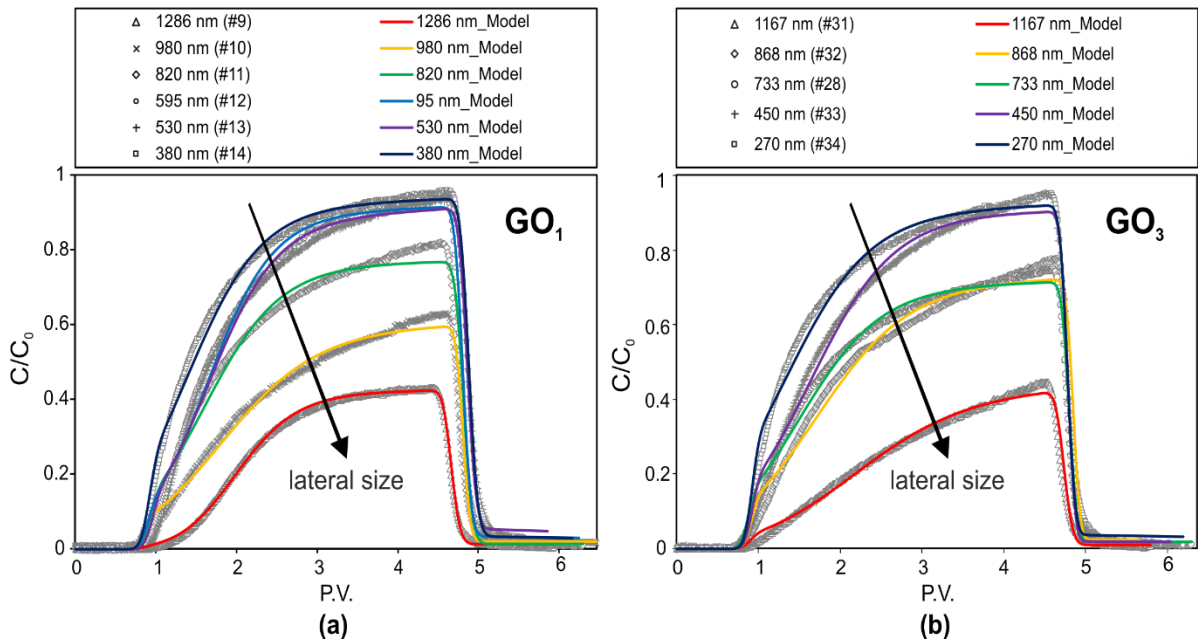
324

### 325        **3.2.1. Effect of lateral size and type of GONP**

326    For a given GO type, the average lateral size was adjusted by tuning the duration of the probe  
327    sonication prior injection, following Figure S8. Figure 1 and Figure 2 report the experimental  
328    and simulated BTCs and the measured retention profiles in columns packed with fine sand  
329    (S<sub>3</sub>) for different lateral sizes of GO<sub>1</sub> (tests no. 6 and 9-14) and GO<sub>3</sub> (test no. 28, 31-34) in the  
330    range 300 to 1300 nm. The results revealed that the GO size strongly affects retention and  
331    transport in saturated sand columns. The mobility of GONP tends to increase with decreasing  
332    particle size. Mass balances (Table S1) indicate that the percentage of retained particles  
333    decreases with decreasing the GO size, consistently with results reported by previous studies  
334    for other types of particles, e.g. the work of Hu et al. (2017) for spherical carbon nanoparticles.  
335    Thus, it suggests that particle shape, for our GONP, has no major influence in this sense.  
336    However, a better insight into retention mechanisms is necessary.

337    Figure 2a shows that larger GO<sub>1</sub> produces strongly declining retention profiles, while smaller  
338    GO<sub>1</sub> produces a more uniform distribution along the column. Previous studies mainly  
339    observed GONP retention to be dominated by physical-chemical interactions with the porous  
340    matrix, resulting in blocking phenomena (Dong et al., 2019; Dong et al., 2016; Dong et al.,  
341    2017; Feriencikova and Xu, 2012; Liu et al., 2013b; Sun et al., 2015; Wang et al., 2018; Xia  
342    et al., 2019). In our study we observed the same behavior for small particles, while for the  
343    largest ones (close to or exceeding 1 micron) the declining retention profiles suggest that  
344    physical retention also plays an important role. Particle size analysis on retained particles  
345    (Figure S11) showed that, for these tests, larger particles are retained close to the column inlet,  
346    and smaller ones travel longer distances; conversely, an almost constant size distribution was  
347    observed when particles significantly smaller than 1 micron were injected.

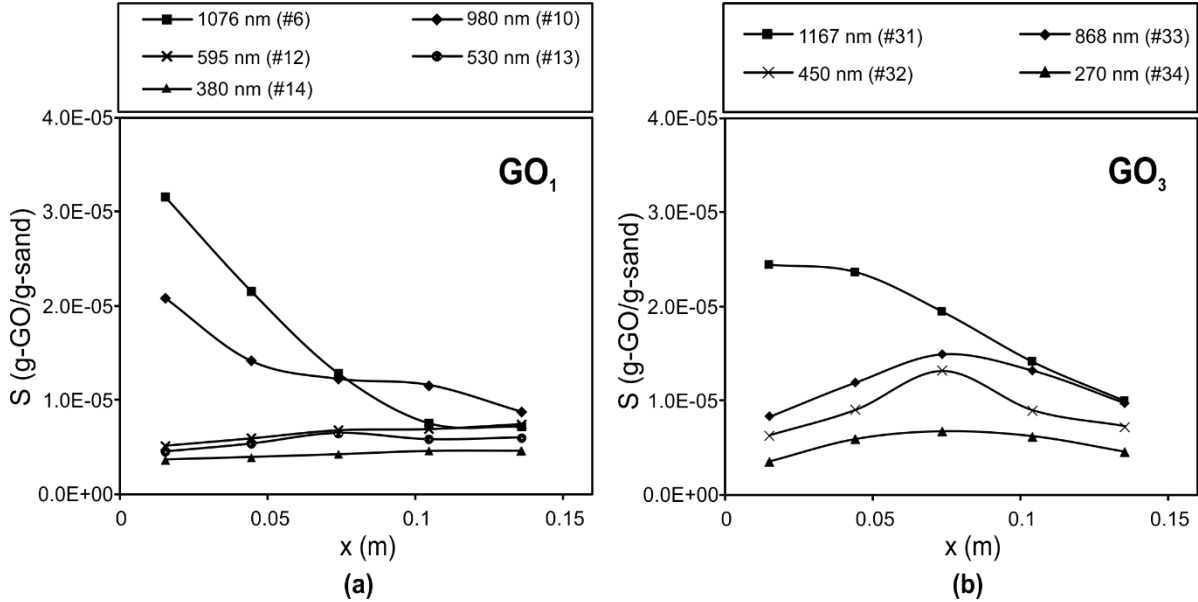
348



349

350 *Figure 1: Observed and simulated breakthrough curves (BTCs) of (a)  $GO_1$  and (b)  $GO_3$  with*  
 351 *different lateral sizes at the same input concentrations of 20 mg/L in Sand  $S_3$ . Symbols:*  
 352 *experimental data/ Lines: simulation results*

353



354

355 *Figure 2: Observed retention profiles of (a)  $GO_1$  and (b)  $GO_3$  with different lateral sizes at*  
 356 *the same input concentrations of 20 mg/L in Sand  $S_3$*

357

358 Likely, the discussed behavior can be attributed to straining. This result is consistent with a  
 359 previous study (Qi et al., 2014a) where the significant straining effect was reported for

360 heterogeneous (natural) saturated porous media. For rounded-shape colloids, it is commonly  
361 accepted that straining is a relevant process if the ratio of particle ( $d_p$ ) to finer sand size ( $d_{10}$ )  
362  $d_p/d_{10} > 0.008$  (Xu et al., 2006). For our sand  $S_3$  (having  $d_{10} = 75 \mu\text{m}$ ) this corresponds to  
363 GONP of approximately 600 nm. As an evidence, clearly declining profiles were observed  
364 for particles of  $1 \mu\text{m}$  or larger, corresponding to a ratio  $d_p/d_{10} \geq 0.013$ .

365 For  $\text{GO}_3$  (Figure 2b) a quite uncommon trend was obtained, with higher retention in the central  
366 portion of the column. This is particularly evident for particles with intermediate size,  
367 probably due to the relatively broad size distribution of these samples (Figure S8 II-b). Similar  
368 non-monotonic trends have been recently attributed to competing deposition of non-  
369 monodispersed colloids in fractures (Malgaresi et al., 2019). This trend was less evident for  
370 the smallest particles (270 nm) with a fairly sharp particle size distribution, which tended to  
371 produce more uniform retention profiles. For the largest ones (1167 nm) instead, a strongly  
372 declining trend was observed due to the predominant effect of straining which masked the  
373 competition effect.

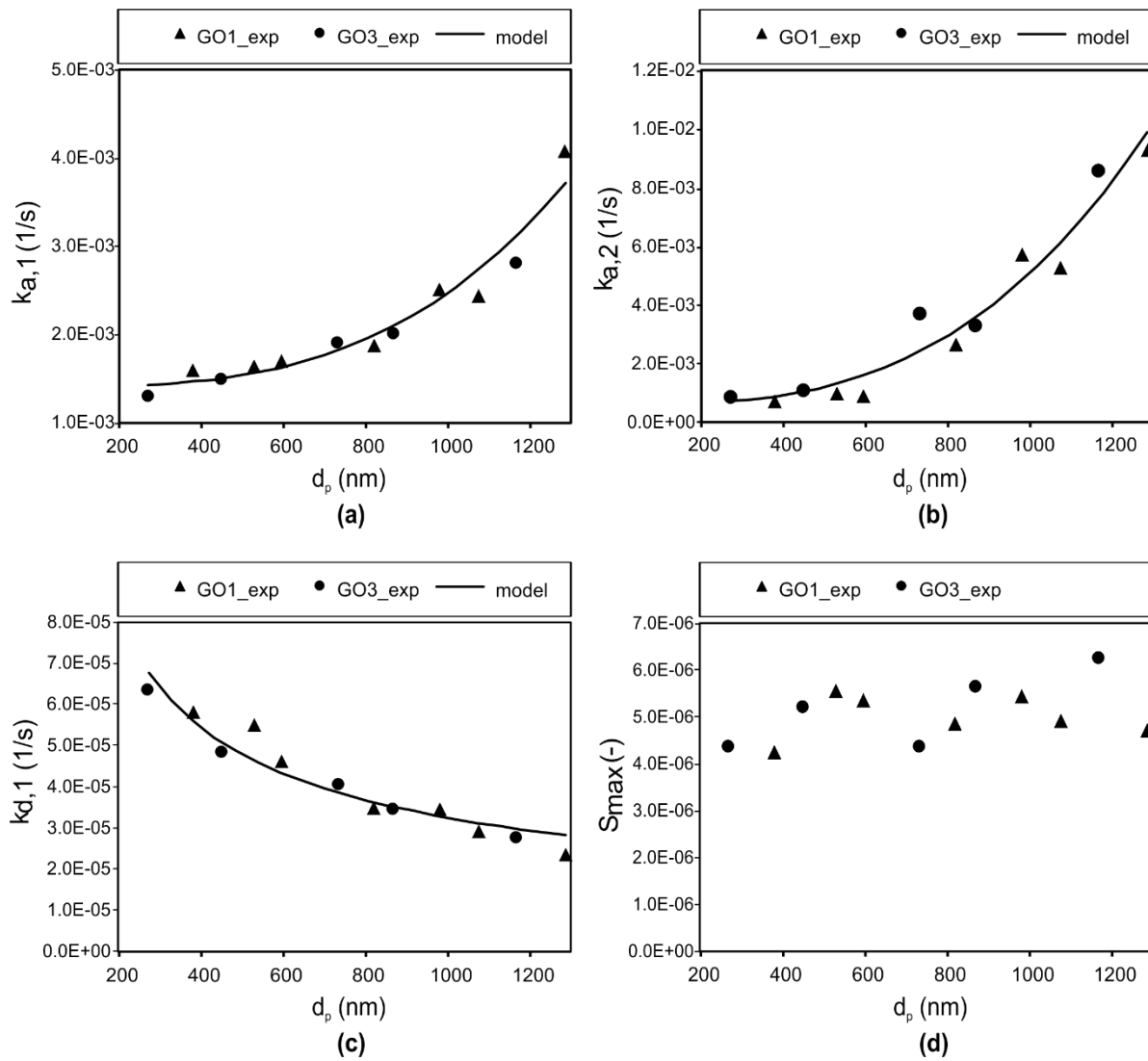
374 The fitted values of the model parameters (namely,  $k_{a,1}$ ,  $S_{\text{max},1}$ ,  $k_{d,1}$ ,  $k_{a,2}$ ) are reported in Table  
375 2 and Figure 3. Fitted values of  $S_{\text{max},1}$  oscillate in the range of  $3.5\text{-}6.0 \cdot 10^{-6} \text{ g/g}$  (Figure 3b),  
376 without any evident correlation between  $S_{\text{max},1}$  and GO lateral size ( $d_p$ ). This range is  
377 comparable with the retained concentrations ( $S$ ) measured for small particles (Figure 2) when  
378 straining does not play a significant role. The attachment kinetics  $k_{a,1}$  and  $k_{a,2}$  both increase  
379 with increasing particle size  $d_p$  (Figure 3a and c). Increasing  $k_{a,1}$  with  $d_p$  means that smaller  
380 GONP attach to the retention site 1 more slowly than larger ones, even if they all tend to reach  
381 a similar saturation concentration. This is also reflected by the different steepness of  
382 breakthrough curves for small particles in Figure 1.

383 Similar to  $k_{a,1}$ , the parameter  $k_{a,2}$  increases with increasing  $d_p$ . For small particles,  $k_{a,1}$  and  $k_{a,2}$   
384 are similar. Conversely, when straining becomes relevant,  $k_{a,2}$  significantly exceeds  $k_{a,1}$  and  
385 retention due to blocking becomes negligible compared to straining. In this case, retention  
386 profiles are strongly declining along the column and breakthrough curves tend to a plateau  
387 concentration  $C/C_0$  lower than 1, which represents an irreversible straining.

388 An empirical power function can be used to model the correlation of the three parameters  
389 ( $k_{a,1}$ ,  $k_{d,1}$  and  $k_{a,2}$ ) with  $d_p$ :

$$k_i = a + b d_p^c \quad (4)$$

390 where  $k_i$  is the generic attachment/detachment kinetic coefficient, and  $a$ ,  $b$ , and  $c$  are fitting  
391 parameters. For  $k_{a,1}$  the fitted values are  $a = 1.41 \cdot 10^{-3} \text{ s}^{-1}$ ,  $b = 3.10 \cdot 10^{15} (\text{s} \cdot \text{m})^{-1}$ ,  $c = 3.077$  with  
392  $R^2 = 0.938$ ; for  $k_{a,2}$   $a = 6.14 \cdot 10^{-4} \text{ s}^{-1}$ ,  $b = 1.20 \cdot 10^{15} (\text{s} \cdot \text{m})^{-1}$ ,  $c = 2.905$  with  $R^2 = 0.947$ ; for  $k_{d,1}$   
393  $a = 4.37 \cdot 10^{-7} \text{ s}^{-1}$ ,  $b = 1.28 \cdot 10^{-8} (\text{s} \cdot \text{m})^{-1}$ ,  $c = -0.567$  with  $R^2 = 0.915$ . The fitted curves are  
394 reported in Figure 3a-c as solid lines. The fitting is satisfactory for all coefficients, with  $R^2$   
395 values above 0.93 in all three cases. It is worth to notice that for all kinetic coefficients the  
396 value represents the lowest, asymptotic kinetics for small (in case of attachment) or large (in  
397 case of detachment) particles. A very similar exponent, close to 3, is found for  $k_{a,1}$  and  $k_{a,2}$ .  
398 The exponent for  $k_{d,1}$  is negative reflecting the declining trend of the detachment kinetics with  
399 increasing particle size.



400

401 *Figure 3: GONP deposition and release coefficients as a function of average particle size*  
 402 *for GO1 and GO3: (a)  $k_{a,1}$  (b)  $k_{a,2}$  (c)  $k_{d,1}$  and (d)  $S_{max}$*

403

404 Interestingly, the results were very close to previous findings obtained for rounded-shaped  
 405 colloids. The obtained trends of  $k_{a,2}$  versus  $d_p$  are consistent with Bradford et al. (2003) who  
 406 reported that a power function can represent a good correlation between  $k_{a,2}$  and particle size  
 407 for latex microparticles. Moreover, the exponent obtained from the detachment kinetic  
 408 coefficient (-0.567) is very close to the theoretical value of -0.58 proposed by Rittman (1982)  
 409 and later adopted by Brovelli et al. (2009) for the detachment of biofilms. However, further

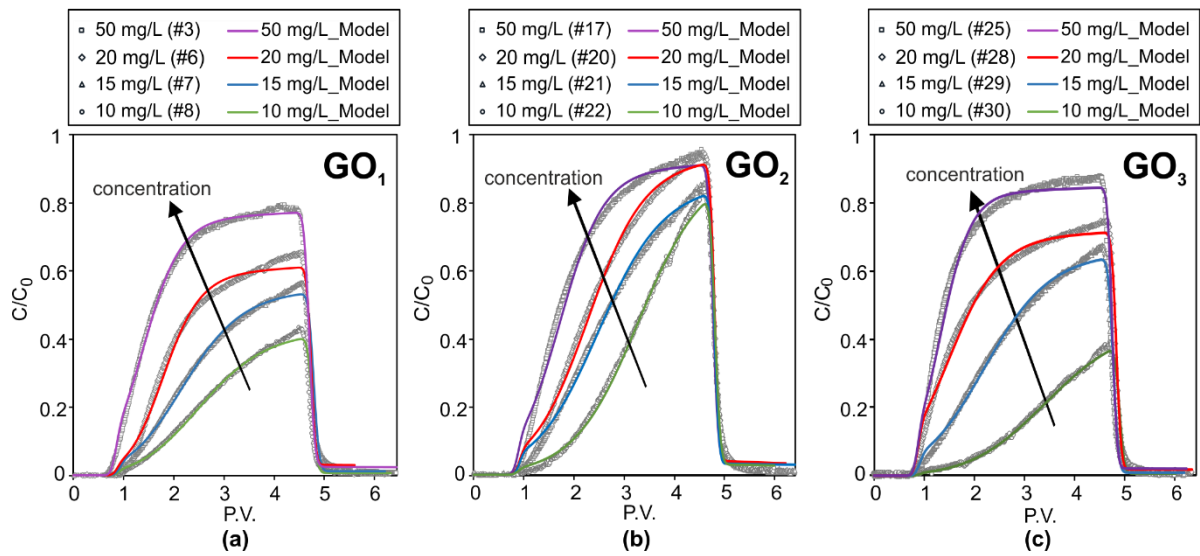
410 studies would be needed to understand if the empirical law of equation 4, or similar power  
411 functions, can be generalized to any type of particles.

### 412 **3.2.2. Effect of input concentration**

413 The transport tests at different input mass concentration ( $C_0$ ) were performed in columns  
414 packed with sand  $S_3$  (tests no. 3 and 6-8 for  $GO_1$ , n. 17 and 20-22 for  $GO_2$ , n. 25 and 28-30  
415 for  $GO_3$ , see Table 2). The GONP size is constant for each test performed with the same GO  
416 type but different sizes were selected for  $GO_1$ ,  $GO_2$ , and  $GO_3$ , in order to have a set of tests  
417 where, respectively, straining is relevant (for  $GO_1$ , average size close to  $1\ \mu\text{m}$ ), is not relevant  
418 ( $GO_2$ , approximately 400 nm) and is expected to play a role, but not to dominate transport  
419 ( $GO_3$ , 700 nm).

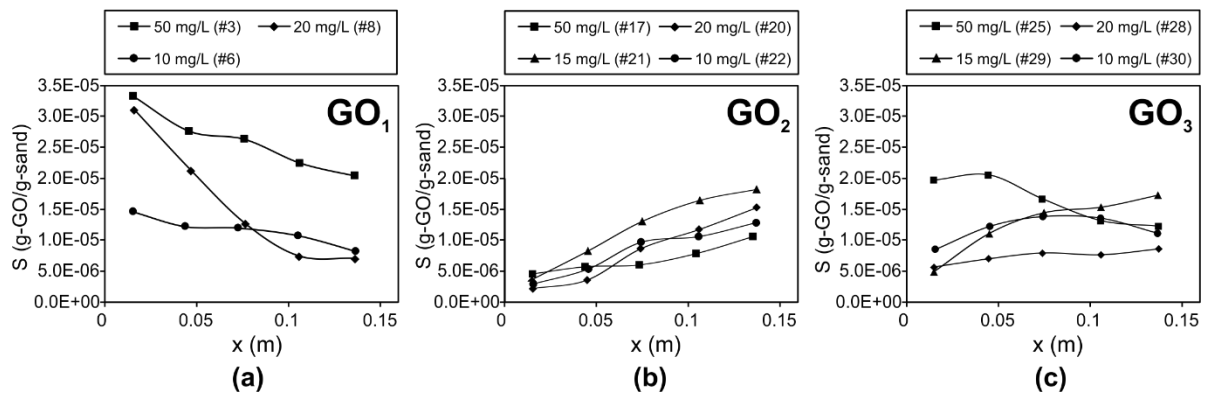
420 The breakthrough curves (Figure 4) show similar trends for all three types of GONP: changing  
421 the input concentration in the range of 10 to 50 mg/L affected the transport and retention of  
422 the nanoparticles. The mobility of all types of GO tends to increase with increasing the  
423 injected concentration  $C_0$ . This finding is consistent with Sun et al. (2015), the only previous  
424 study, to our knowledge, investigating the influence of inlet concentration on the transport  
425 and retention of GONP. Mass balance and mass recovery calculations (Table S1) confirm that  
426 the total retained mass decreases with increasing  $C_0$ . The observed behavior is coherent with  
427 blocking-dominated deposition. In other words, a higher  $C_0$  saturates the deposition sites more  
428 rapidly compared with lower  $C_0$ , thus increasing the overall mobility of the injected  
429 suspension. Our tests with higher  $C_0$  show a steeper increase of the breakthrough curves, even  
430 if the effect is less pronounced for  $GO_2$ , which is the sample with the overall highest mobility  
431 and smallest particle size. It is noteworthy that some differences exist among the GO types.  
432 However, based on the results discussed in the previous paragraph, it can be assumed that

433 these differences are related mainly to the different size of the three samples, rather than to  
 434 possible minor differences in composition and surface properties.



435  
 436 *Figure 4: Observed and simulated breakthrough curves (BTCs) of (a)GO<sub>1</sub> (Z-Ave. 1050±100 nm), (b)*  
 437 *GO<sub>2</sub> (Z-Ave. 410±50 nm), and (c) GO<sub>3</sub> (Z-Ave. 650±100 nm) at different input concentrations from*  
 438 *50 mg/L to 10 mg/L in sand S<sub>3</sub>. Symbols: experimental data/ Lines: simulation results*

439



440  
 441 *Figure 5: Observed retention profiles of (a) GO<sub>1</sub>, (b) GO<sub>2</sub>, and (c) GO<sub>3</sub> at different input*  
 442 *concentrations from 50 mg/L to 10 mg/L in sand S<sub>3</sub>.*

443

444 Considering the modeling of GONP transport, the fitting obtained is satisfactory for all  
 445 breakthrough curves. For GO<sub>1</sub> and GO<sub>3</sub>, the two-site deposition model correctly describes the  
 446 GO transport. Conversely, for GO<sub>2</sub>, characterized by the smallest particle size, straining is

447 irrelevant for all tests except those where the highest concentration (50 mg/L) is injected. This  
448 suggests that, in such conditions, a stronger interaction arises between deposited particles and  
449 those suspended in the pore water, promoting enhanced deposition processes.

450 The attachment and detachment kinetic coefficients  $k_{a,1}$  and  $k_{d,1}$  do not significantly change  
451 with changing injected concentration. Conversely, a slight increase of  $S_{max,1}$  with increasing  
452 injected concentration is observed, even if the explanation for this is unclear, and further  
453 investigation would be needed to elucidate this aspect.

454

### 455 **3.2.3. Effect of sand grain size**

456 Figure 6 depicts the experimental and simulated BTCs of  $GO_1$  (tests n. 1-6 in Table 2) injected  
457 at 20 and 50 mg/L in sands  $S_1$  (coarse),  $S_2$  (medium) and  $S_3$  (fine). The corresponding  
458 retention profiles are reported in Figure 7. Also, for this set of tests, the size of the three GO  
459 samples was adjusted to approximately 1  $\mu\text{m}$  for  $GO_1$ , 400 nm for  $GO_2$  and 700 nm for  $GO_3$ .

460 The results indicate that the sand grain size significantly affects the transport and retention of  
461 GONP. The same tests performed using  $GO_2$  (tests 15-20 in Table 2) and  $GO_3$  (tests 23-28 in  
462 Table 2) are reported in the Supporting Information (Figure S13) and show similar results.  
463 The impact of sand size on the transport of  $GO_2$  and  $GO_3$  showed similar results.

464 As a general outcome, the mobility of GONP at a given  $C_0$  tends to increase with increasing  
465 the sand grain size. The highest breakthrough concentration is found in coarse sand. The  
466 corresponding retention profile is almost constant along the column, thus indicating that  
467 straining is limited or even negligible. Conversely, reducing the grain size, the breakthrough  
468 decreases, and straining becomes more relevant. The mass balances (Table 1) confirm that

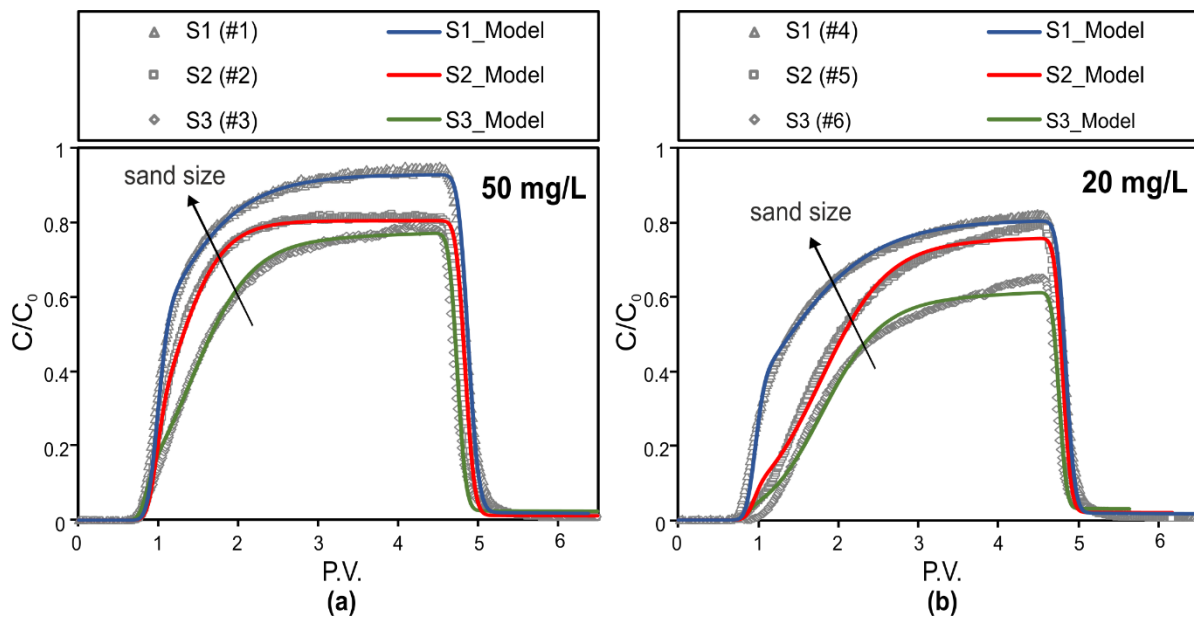
469 decreasing the sand size lead the total retention to significantly increase for all GO types and  
470 both injected concentrations.

471 The fitted parameters reported in Table 2 indicate how changing the sand size affects the  
472 relative importance of blocking and straining retention mechanisms. As for physical-chemical  
473 deposition following the blocking dynamics, the attachment kinetic coefficient  $k_{a,1}$  increases  
474 with decreasing sand size (from  $S_1$  to  $S_3$ ), and coherently  $k_{d,1}$  decreases for both injected  
475 concentrations. This was expected from the established literature on colloid removal  
476 efficiency in granular media (Messina et al., 2016; Sun et al., 2015; Tufenkji and Elimelech,  
477 2004; Yao et al., 1971). Some other experimental studies investigating the effect of the grain  
478 size on the particle attachment rate (Bradford and Bettahar, 2006; Kasel et al., 2012; Liang et  
479 al., 2013; Sun et al., 2015; Torkzaban et al., 2010) achieved the similar results, even if the  
480 great majority of such studies focused on spherical colloidal particles, e.g. carboxyl latex,  
481 QDs, and AgNPs.

482 Differences in the maximum retainable concentration due to physico-chemical interactions  
483 ( $S_{max,1}$ ) among the three sand samples are attributable to differences in SSA, since no  
484 significant difference in zeta potential was observed. As a general rule, the fitted values of  
485  $S_{max,1}$  (Table 2) increase with decreasing sand size (i.e. from  $S_1$  to  $S_3$ ) for a given GO type and  
486 injected concentration; this results in  $S_{max,1}$  values for  $S_3$  approximately two times higher than  
487 the  $S_{max,1}$  obtained for  $S_1$ , in agreement with SSA of sand grains (assuming spherical grains,  
488 SSA for  $S_1$  and  $S_3$  is respectively 0.008 and 0.003 m<sup>2</sup>/kg, being the average grain size 0.75  
489 and 0.28 mm).

490 Straining also contributed to the retention of GONP and affected the shape of profiles of  
491 retained particles. Based on the considerations discussed in the previous paragraphs, straining  
492 is expected to occur for  $GO_1$  and, limitedly, for  $GO_2$ . Back again to the ratio  $d_p/d_{10}$  and the

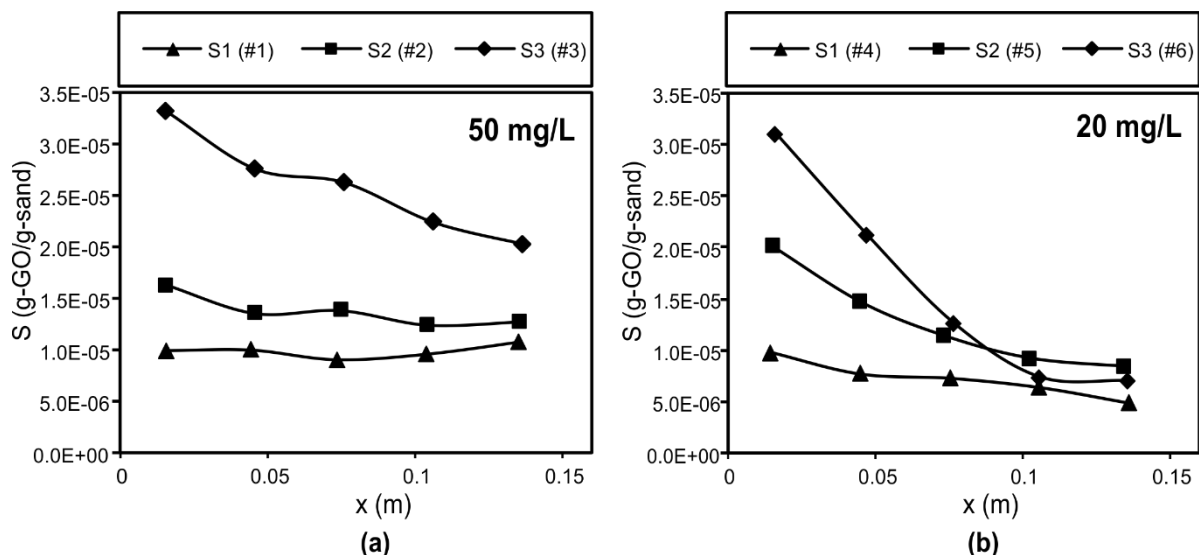
493 straining limit of 0.008 (Xu et al., 2006),  $GO_1$  was expected to exceed this threshold value in  
 494 sand  $S_3$ , and to approach the limit for  $S_2$ . Coherently, the retention profiles (Figure 7) showed  
 495 a steep decrease for  $S_3$  and a less pronounced decrease for  $S_2$ . The fitted straining coefficients  
 496  $k_{a,2}$  are lower for coarse sand and increase with decreasing sand size. Changes in  $k_{a,2}$  from  $S_1$   
 497 to  $S_3$  cover approximately one order of magnitude (typically from  $10^{-4} \text{ s}^{-1}$  to  $10^{-3} \text{ s}^{-1}$ ) and are  
 498 more evident at the highest injected concentration (for example, compare the values of  $k_{a,2}$  for  
 499  $GO_1$  and  $GO_3$  injected at 50 mg/L).



500

501 *Figure 6: Observed and simulated breakthrough curves for  $GO_1$ , injected in columns*  
 502 *packed with sand  $S_1$ ,  $S_2$ , and  $S_3$  at a concentration of 50 mg/L and 20 mg/L.*

503



504

505 *Figure 7: Observed retention profiles of GO<sub>1</sub> with two different input concentrations of (a)*  
 506 *50 mg/L and (b) 20 mg/L in various sand sizes of S<sub>1</sub> (coarse), S<sub>2</sub> (medium), and S<sub>3</sub> (fine).*

507

#### 508 **4. Conclusions**

509 This study showed that GONP can be stably dispersed in water and are remarkably mobile  
 510 when injected in silica sand. The experimental results also showed that a parameter having a  
 511 major impact on GONP mobility is the particle lateral size; also the size ratio of particle to  
 512 sand grains is relevant. Conversely, the source of graphene oxide (i.e. synthesized in the  
 513 laboratory or provided by commercial producers) had a minor impact, even if the C and O  
 514 content of the three GONP types was not identical. This suggests that the outcomes of this  
 515 study could potentially be extended also to other GONP not considered here. The injected  
 516 concentration affected the mobility of the particles but, at least in the range herein explored,  
 517 has had no dramatic effect.

518 Despite the peculiar shape of GONP compared to more conventional colloids, the advection-  
 519 dispersion-deposition equation commonly used for colloid transport in porous media was still  
 520 adequate to describe the transport of these particles. The experimental and modeling results  
 521 indicated that both physico-chemical (blocking) and physical (straining) retention

522 mechanisms strongly influence the transport and retention of GONP. Blocking is observed in  
523 all cases and is coherent with the good colloidal stability of the particles. Straining becomes  
524 relevant for larger particles and/or finer sand, as expected from round-shaped colloids, and  
525 plays a relevant role only for particles exceeding approximately 0.5-1% of the sand  $d_{10}$ .  
526 Therefore, the retention associated to the physical interaction of GONP with the porous  
527 medium cannot be neglected.

528 Concerning the potential application to groundwater remediation, the results of this study are  
529 very promising. GONP are sufficiently mobile to expect a relatively easy injection in the field,  
530 and the possibility to control their migration and deposition in the subsoil by modifying the  
531 particle size.

532

## 533 **5. Acknowledgments**

534 Authors would like to acknowledge prof. Matteo Pavese (DISAT – Politecnico di Torino) and  
535 his group for the support in graphene oxide synthesis, and the personnel of laboratories at  
536 DIATI - Politecnico di Torino and of the Department of Civil and Environment, Polytechnic  
537 University of Tehran (Amirkabir) for their appreciated help with experiments and chemical  
538 analyses. The work was conducted in the laboratories of Politecnico di Torino and was partly  
539 supported by Iran National Science Foundation (INSF) [grant number 95815221] and Iran  
540 Nanotechnology Initiative Council (INIC) [grant number 107029].

541

## 542 **6. Competing interests statement**

543 The authors have no competing interests

544

545

- 547 Akpotu SO, Moodley B. Application of as-synthesised MCM-41 and MCM-41 wrapped with reduced graphene  
548 oxide/graphene oxide in the remediation of acetaminophen and aspirin from aqueous system. *Journal of*  
549 *Environmental Management* 2018; 209: 205-215.
- 550 Bianco C, Tosco T, Sethi R. A 3-dimensional micro- and nanoparticle transport and filtration model (MNM3D) applied to  
551 the migration of carbon-based nanomaterials in porous media. *Journal of Contaminant Hydrology* 2016; 193: 10-  
552 20.
- 553 Bradford SA, Bettahar M. Concentration dependent transport of colloids in saturated porous media. 2006; 82: 99-117.
- 554 Bradford SA, Bettahar M, Simunek J, van Genuchten MT. Straining and Attachment of Colloids in Physically Heterogeneous  
555 Porous Media. *Vadose Zone Journal* 2004; 3: 384-394.
- 556 Bradford SA, Kim HN, Haznedaroglu BZ, Torkzaban S, Walker SL. Coupled Factors Influencing Concentration-Dependent  
557 Colloid Transport and Retention in Saturated Porous Media. 2009; 43: 6996-7002.
- 558 Bradford SA, Simunek J, Bettahar M, Van Genuchten MT, Yates SR. Modeling Colloid Attachment, Straining, and  
559 Exclusion in Saturated Porous Media. 2003.
- 560 Brovelli A, Malaguerra F, Barry DA. Bioclogging in porous media: Model development and sensitivity to initial conditions.  
561 *Environmental Modelling & Software* 2009; 24: 611-626.
- 562 Camesano TA, Logan BE. Influence of Fluid Velocity and Cell Concentration on the Transport of Motile and Nonmotile  
563 Bacteria in Porous Media. 1998: 1699-1708.
- 564 Chen D, Feng H, Li J. Graphene oxide: preparation, functionalization, and electrochemical applications. *Chem Rev* 2012;  
565 112: 6027-53.
- 566 Chen J, Yao B, Li C, Shi G. An improved Hummers method for eco-friendly synthesis of graphene oxide. *Carbon* 2013; 64:  
567 225-229.
- 568 Chrysikopoulos CV, Sotirelis NP, Kallithrakas-Kontos NG. Cotransport of Graphene Oxide Nanoparticles and Kaolinite  
569 Colloids in Porous Media. *Transport in Porous Media* 2017; 119: 181-204.
- 570 Corsi I, Winther-nielsen M, Sethi R, Punta C, Torre CD, Libralato G, et al. Ecofriendly nanotechnologies and nanomaterials  
571 for environmental applications : Key issue and consensus recommendations for sustainable and ecosafe  
572 nanoremediation. *Ecotoxicology and Environmental Safety* 2018; 154: 237-244.
- 573 Dong S, Gao B, Sun Y, Guo H, Wu J, Cao S, et al. Visualization of graphene oxide transport in two-dimensional  
574 homogeneous and heterogeneous porous media. *Journal of Hazardous Materials* 2019; 369: 334-341.
- 575 Dong S, Shi X, Gao B, Wu J, Sun Y, Guo H, et al. Retention and Release of Graphene Oxide in Structured Heterogeneous  
576 Porous Media under Saturated and Unsaturated Conditions. *Environmental Science & Technology* 2016; 50:  
577 10397-10405.
- 578 Dong S, Sun Y, Gao B, Shi X, Xu H, Wu J, et al. Retention and transport of graphene oxide in water-saturated limestone  
579 media. *Chemosphere* 2017; 180: 506-512.
- 580 Fan W, Jiang X, Lu Y, Huo M, Lin S, Geng Z. Effects of surfactants on graphene oxide nanoparticles transport in saturated  
581 porous media. *Journal of Environmental Sciences (China)* 2015a; 35: 12-19.
- 582 Fan W, Jiang XH, Yang W, Geng Z, Huo MX, Liu ZM, et al. Transport of graphene oxide in saturated porous media: Effect  
583 of cation composition in mixed Na–Ca electrolyte systems. *Science of The Total Environment* 2015b; 511: 509-  
584 515.
- 585 Feriencikova L, Xu S. Deposition and remobilization of graphene oxide within saturated sand packs. *Journal of Hazardous*  
586 *Materials* 2012; 235-236: 194-200.
- 587 Godinez IG, Darnault CJG. Aggregation and transport of nano-TiO<sub>2</sub> in saturated porous media: Effects of pH, surfactants  
588 and flow velocity. *Water Research* 2011; 45: 839-851.
- 589 Hosseini SM, Tosco T. Transport and retention of high concentrated nano-Fe/Cu particles through highly flow-rated packed  
590 sand column. *Water Research* 2013; 47: 326-338.
- 591 Hu Z, Zhao J, Gao H, Nourafkan E, Wen D, Hu Z, et al. Transport and Deposition of Carbon Nanoparticles in Saturated  
592 Porous Media. *Energies* 2017; 10: 1151.
- 593 Huang X, Yin Z, Wu S, Qi X, He Q, Zhang Q, et al. Graphene-based materials: Synthesis, characterization, properties, and  
594 applications. *Small* 2011; 7: 1876-1902.
- 595 Iqbal MZ, Abdala AA. Oil spill cleanup using graphene. 2013: 3271-3279.
- 596 Jian-Zhou H, Cheng-Cheng L, Deng-Jun W, Zhou D-M. Biofilms and extracellular polymeric substances mediate the  
597 transport of graphene oxide nanoparticles in saturated porous media. *Journal of Hazardous Materials* 2015; 300:  
598 467-474.
- 599 Jiang Y, Zhang X, Yin X, Sun H, Wang N. Graphene oxide-facilitated transport of Pb<sup>2+</sup> and Cd<sup>2+</sup> in saturated porous media.  
600 *Science of the Total Environment* 2018; 631-632: 369-376.
- 601 Johnson PR, Sun N, Elimelech M. Colloid transport in physically and geochemically heterogeneous porous media\_  
602 Modeling, measurements, and parameter identification.pdf. *Environmental Science and Technology* 1996; 30:  
603 3284-3293.
- 604 Karn B, Kuiken T, Otto M. Nanotechnology and in Situ Remediation : A Review of the Benefits and. 2009; 117: 1823-1831.
- 605 Kasel D, Bradford SA, Klumpp E, Gru P. Transport and retention of multi-walled carbon nanotubes in saturated porous  
606 media : Effects of input concentration and grain size. 2012; 7.
- 607 Lanphere JD, Luth CJ, Walker SL. Effects of Solution Chemistry on the Transport of Graphene Oxide in Saturated Porous  
608 Media. *Environmental Science & Technology* 2013; 47: 4255-4261.

609 Lanphere JD, Rogers B, Luth C, Bolster CH, Walker SL. Stability and Transport of Graphene Oxide Nanoparticles in  
610 Groundwater and Surface Water. *Environ Eng Sci* 2014; 31: 350-359.

611 Li Y, Yang N, Du T, Wang X, Chen W. Transformation of graphene oxide by chlorination and chloramination: Implications  
612 for environmental transport and fate. *Water Res* 2016; 103: 416-423.

613 Liang Y, Bradford SA, Simunek J, Vereecken H, Klumpp E. Sensitivity of the transport and retention of stabilized silver  
614 nanoparticles to physicochemical factors. *Water Research* 2013; 47: 2572-2582.

615 Liu J, Cui L, Losic D. Graphene and graphene oxide as new nanocarriers for drug delivery applications. *Acta Biomaterialia*  
616 2013a; 9: 9243-9257.

617 Liu L, Gao B, Wu L, Morales VL, Yang L, Zhou Z, et al. Deposition and transport of graphene oxide in saturated and  
618 unsaturated porous media. *Chemical Engineering Journal* 2013b; 229: 444-449.

619 Liu L, Gao B, Wu L, Yang L, Zhou Z, Wang H. Effects of pH and surface metal oxyhydroxides on deposition and transport  
620 of carboxyl-functionalized graphene in saturated porous media. *Journal of Nanoparticle Research* 2013c; 15.

621 Lotya M, Rakovich A, Donegan JF, Coleman JN. Measuring the lateral size of liquid-exfoliated nanosheets with dynamic  
622 light scattering. *Nanotechnology* 2013; 24.

623 Lu T, Xia T, Qi Y, Chengdong Z, Chen W. Effect of clay materials on transport of graphene oxide in saturated porous media.  
624 2017; 36: 655-660.

625 Malgaresi G, Collins B, Alvaro P, Bedrikovetsky P. Explaining non-monotonic retention profiles during flow of size-  
626 distributed colloids. *Chemical Engineering Journal* 2019; 375: 121984.

627 Messina F, Tosco T, Sethi R. On the failure of upscaling the single-collector efficiency to the transport of colloids in an array  
628 of collectors. *Water Resources Research* 2016; 52: 5492-5505.

629 Montes-Navajas P, Asenjo NG, Santamaría R, Menéndez R, Corma A, García H. Surface area measurement of graphene  
630 oxide in aqueous solutions. *Langmuir* 2013; 29: 13443-13448.

631 Novoselov KS, Fal VI, Colombo L, Gellert PR, Schwab MG, Kim K. REVIEW A roadmap for graphene. *Nature* 2012; 490:  
632 192-200.

633 O'Carroll D, Sleep B, Krol M, Boparai H, Kocur C. Nanoscale zero valent iron and bimetallic particles for contaminated site  
634 remediation. *Advances in Water Resources* 2013; 51: 104-122.

635 Patil SS, Shedbalkar UU, Truskewycz A, Chopade BA, Ball AS. Environmental Technology & Innovation Nanoparticles for  
636 environmental clean-up : A review of potential risks and emerging solutions. *Environmental Technology &*  
637 *Innovation* 2016; 5: 10-21.

638 Paulchamy B, Arthi G, Lignesh B. A Simple Approach to Stepwise Synthesis of Graphene Oxide Nanomaterial. *Journal of*  
639 *Nanomedicine & Nanotechnology* 2015; 06: 2-5.

640 Peng S, Wu D, Ge Z, Tong M, Kim H. Influence of graphene oxide on the transport and deposition behaviors of colloids in  
641 saturated porous media. *Environmental Pollution* 2017; 225: 141-149.

642 Qi Z, Zhang L, Chen W. Transport of graphene oxide nanoparticles in saturated sandy soil. *Environmental Sciences:*  
643 *Processes and Impacts* 2014a; 16: 2268-2277.

644 Qi Z, Zhang L, Wang F, Hou L, Chen W. Factors controlling transport of graphene oxide nanoparticles in saturated sand  
645 column. 2014b; 33: 998-1004.

646 Rittman BE. The effect of shear stress on biofilm loss rate. *Biotechnology and Bioengineering* 1982; 24: 501-506.

647 Shahriary L, Athawale AA. Graphene Oxide Synthesized by using Modified Hummers Approach. *International Journal of*  
648 *Renewable Energy and Environmental Engineering* 2014; 02: 58-63.

649 Sun L, Yu H, Fugetsu B. Graphene oxide adsorption enhanced by in situ reduction with sodium hydrosulfite to remove  
650 acridine orange from aqueous solution. *Journal of Hazardous Materials* 2012; 203-204: 101-110.

651 Sun Y, Gao B, Bradford SA, Wu L, Chen H, Shi X, et al. Transport, retention, and size perturbation of graphene oxide in  
652 saturated porous media: Effects of input concentration and grain size. *Water Research* 2015; 68: 24-33.

653 Torkzaban S, Kim Y, Mulvihill M, Wan J, Tokunaga TK. Transport and deposition of functionalized CdTe nanoparticles in  
654 saturated porous media. *Journal of Contaminant Hydrology* 2010; 118: 208-217.

655 Tortello M, Colonna S, Bernal M, Gomez J, Pavese M, Novara C, et al. Effect of thermal annealing on the heat transfer  
656 properties of reduced graphite oxide flakes: A nanoscale characterization via scanning thermal microscopy. *Carbon*  
657 2016; 109: 390-401.

658 Tosco T, Bosch J, Meckenstock RU, Sethi R. Transport of ferrihydrite nanoparticles in saturated porous media: Role of ionic  
659 strength and flow rate. *Environmental Science and Technology* 2012; 46: 4008-4015.

660 Tosco T, Petrangeli M, Cruz C, Sethi R. Nanoscale zerovalent iron particles for groundwater remediation : a review. *Journal*  
661 *of Cleaner Production* 2014; 77: 10-21.

662 Tosco T, Sethi R. Transport of non-newtonian suspensions of highly concentrated micro- and nanoscale iron particles in  
663 porous media: A modeling approach. *Environmental Science and Technology* 2010; 44: 9062-9068.

664 Tosco T, Tiraferri A, Sethi R. Ionic Strength Dependent Transport of Microparticles in Saturated Porous Media: Modeling  
665 Mobilization and Immobilization Phenomena under Transient Chemical Conditions. *Environmental Science &*  
666 *Technology* 2009; 43: 4425-4431.

667 Tufenkji N, Elimelech M. Correlation Equation for Predicting Single-Collector Efficiency in Physicochemical Filtration in  
668 Saturated Porous Media. 2004; 38: 529-536.

669 Wang C, Bobba AD, Attinti R, Shen C, Lazouskaya V, Wang L-P, et al. Retention and Transport of Silica Nanoparticles in  
670 Saturated Porous Media: Effect of Concentration and Particle Size. 2012.

671 Wang D, Paradelo M, Bradford SA, Peijnenburg WJGM, Chu L, Zhou D. Facilitated transport of Cu with hydroxyapatite  
672 nanoparticles in saturated sand: Effects of solution ionic strength and composition. *Water Research* 2011; 45: 5905-  
673 5915.

674 Wang M, Gao B, Tang D, Sun H, Yin X, Yu C. Effects of temperature on graphene oxide deposition and transport in saturated  
675 porous media. *J Hazard Mater* 2017; 331: 28-35.

676 Wang M, Gao B, Tang D, Yu C. Concurrent aggregation and transport of graphene oxide in saturated porous media : Roles  
677 of temperature , cation type , and electrolyte. *Environmental Pollution* 2018; 235: 350-357.

678 Xia T, Qi Y, Zhu L, Qi Z, Chen W. Transport and retention of reduced graphene oxide materials in saturated porous media  
679 : Synergistic effects of enhanced attachment and particle aggregation \*. 2019; 247: 383-391.

680 Xu S, Gao B, Saiers JE. Straining of colloidal particles in saturated porous media. *Water Resources Research* 2006; 42.

681 Yang X, Li J, Wen T, Ren X, Huang Y, Wang X. *Colloids and Surfaces A : Physicochemical and Engineering Aspects*  
682 Adsorption of naphthalene and its derivatives on magnetic graphene composites and the mechanism investigation.  
683 *Colloids and Surfaces A: Physicochemical and Engineering Aspects* 2013; 422: 118-125.

684 Yao K-M, Habibian MT, O'Melia CR. *Water and Waste Water Filtration: Concepts and Applications.* 1971; 5: 1105-1112.

685 Yin X, Jiang Y, Tan Y, Meng X, Sun H, Wang N. Co-transport of graphene oxide and heavy metal ions in surface-modified  
686 porous media. *Chemosphere* 2019; 218: 1-13.

687 Zhang W, Morales VnL, Cakmak ME, Salvucci AE, Geohring LD, Hay AG, et al. Colloid Transport and Retention in  
688 Unsaturated Porous Media: Effect of Colloid Input Concentration. *Environmental Science & Technology* 2010;  
689 44: 4965-4972.

690 Zhao K, Chen C, Cheng T, Shang J. Graphene oxide-facilitated uranium transport and release in saturated medium : Effect  
691 of ionic strength and medium structure. *Environmental Pollution* 2019; 247: 668-677.

692 Zhou DD, Jiang XH, Lu Y, Fan W, Huo MX, Crittenden JC. Cotransport of graphene oxide and Cu(II) through saturated  
693 porous media. *Science of the Total Environment* 2016; 550: 717-726.

694